

Supramolecular Assemblies of Polyaniline through Cooperative Bundling by a Palladium-Complex-Appended Synthetic Cross-Linker

Takahiro Kaseyama,^[a, b, c] Shinji Takebayashi,^[b] Rie Wakabayashi,^[b] Seiji Shinkai,^{*,[b]}
Kenji Kaneko,^[d] and Masayuki Takeuchi^{*,[a, c]}

Abstract: A synthetic cross-linker (**1**) bearing two binding sites for imine moieties in polyaniline has been used to organize polyaniline emeraldine base (**EB**) or polyaniline emeraldine salt (**ES**) into aligned assemblies. Complex **1** exhibited highly cooperative binding toward **mEB** (a repeating unit analogue of **EB**), for which the association constants K_1 and K_2 were evaluated to be 2.2×10^4 and $9.4 \times 10^5 \text{ M}^{-1}$, respectively. ^1H NMR studies revealed

that the diimine moieties in **mEB** are recognized cooperatively in *anti*-conformation by **1**. The ordered structures organized from **1** and **EB** or **ES** were efficiently formed through supramolecular bundling. These ordered assemblies have a periodicity of 2.5 nm that

Keywords: allostherism • conjugation • palladium • polyaniline • polymers • supramolecular chemistry

was confirmed by means of transmittance electron microscopy (TEM) and high-resolution TEM (HRTEM). The cooperative binding would be important for the bundling and alignment of the polymers, as evidenced by the fact that neither reference compounds **2** nor **3** were capable of producing similar assemblies. The electric conductivity of the samples was measured and the results were discussed.

Introduction

Conductive polymers have attracted considerable attention because of their mechanical flexibility, light weight, and electronic and photonic properties.^[1] They have potential for

application to rechargeable batteries, electrochromic devices, capacitors, field-effect transistors, light-emitting diodes, solar cells, and so forth.^[2–5] In particular, polyaniline (PANI) is one of the most extensively studied conducting polymers to date, due to its ease of synthesis by chemical and electrochemical polymerization, chemical stability, and inexpensiveness.^[6,7] Poor processability and low solubility into common organic solvents, however, would be the bottleneck for its commercial applications. Many attempts to manipulate PANI in organic or aqueous solvents have been carried out by many research groups and they can be categorized into three approaches. The first approach is a synthetic one; for example, the introduction of side chains into the PANI main chain, such as poly(*o*-toluidine).^[8] The second approach is the use of ion complexation of surfactant anions with protonated PANI. Dodecylbenzenesulfonic acid, camphor sulfonic acid (CSA), and other sulphonic acids bearing long alkyl chains are often employed as the surfactant anion;^[9] although they are not perfectly dissolved into solvents, but are instead dispersed uniformly or organized into fine structures. The third one is a supramolecular method, in which PANI is incorporated into cyclodextrin, cucurbituril, and biomolecules.^[10] The resultant composites are homogeneously soluble in solvents. In these approaches, it is of importance to segregate polymers into individual chains and to control the alignment of PANI with defined conformation

[a] T. Kaseyama, Prof. M. Takeuchi
Macromolecules Group
Organic Nanomaterials Center
National Institute for Materials Science
Tsukuba 305-0047 (Japan)
Fax: (+81)29-859-2101
Takeuchi.Masayuki@nims.go.jp

[b] T. Kaseyama, Dr. S. Takebayashi, Dr. R. Wakabayashi,
Prof. S. Shinkai
Department of Chemistry and Biochemistry
Graduate School of Engineering
Kyushu University, Fukuoka 819-0395 (Japan)

[c] T. Kaseyama, Prof. M. Takeuchi
Department of Materials Science and Engineering
Graduate School of Pure and Applied Science
Tsukuba University, Tsukuba 305-0047 (Japan)

[d] Prof. K. Kaneko
HVEM Laboratory, Kyushu University
Fukuoka 819-0395 (Japan)

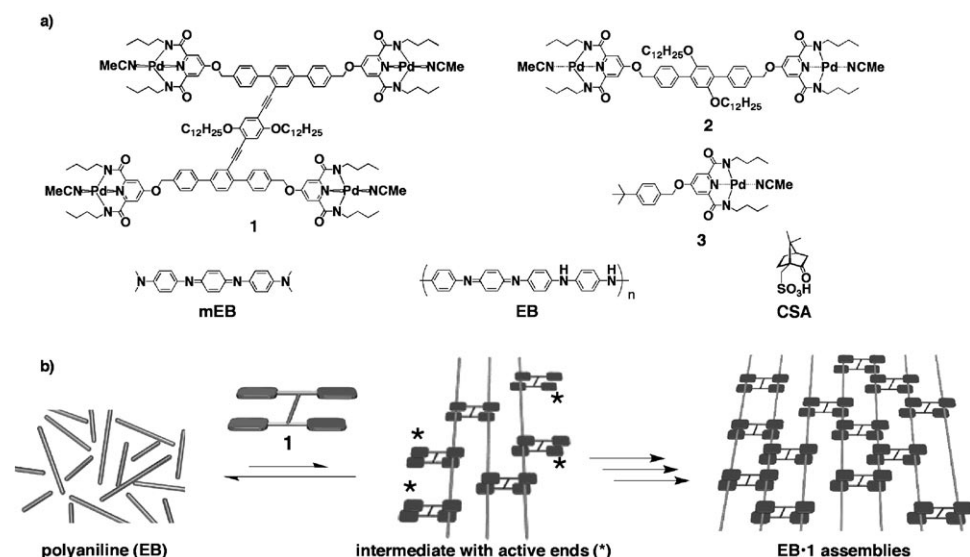
Supporting information for this article is available on the WWW under <http://dx.doi.org/10.1002/chem.200902305>.

and arrangement for the production of PANI-based devices.^[11]

Recently we reported a new concept for aligning and assembling conjugated polymers through the action of supramolecular cross-linking molecules (aligner).^[12,13] The concept was inspired by the action of bundling proteins in animal cells, in which one-dimensional (1D) actin filaments are cross-linked to form aligned bundles and the distinct properties of bundling proteins determine the types of assemblies.^[12c] We demonstrated this concept by utilizing the coordination bonds formed between porphyrinatozinc and amine-functionalized poly(phenylene ethynylene) (PPE) derivatives, which contribute to the high affinity and distinct bonding geometry of these species. In addition, we applied a dynamic molecular recognition concept—positive homotropic allosterism—to this system. In positive allosteric systems, the recognition of the first guest molecule facilitates the subsequent binding of the other guests. For the binding of conjugated polymers, the first binding event enhances the second one to form aligned supramolecular assemblies. Such a process would be indispensable to avoid the formation of random, disordered assemblies. As a result, these binding events enable 1D polymers to form supramolecular two-dimensional (2D) polymer structures.^[14] It occurred to us that our recent finding regarding aligner molecules could be applied to the alignment of polyaniline to prepare crystalline sheet structures. In this paper, as one of the post-alignment schemes, we report that compound **1** cooperatively cross-links polyaniline emeraldine base (**EB**) and polyaniline emeraldine salt (**ES**) to form ordered structures with periodicity of 2.5 nm through a supramolecular bundling (Scheme 1).

Results and Discussion

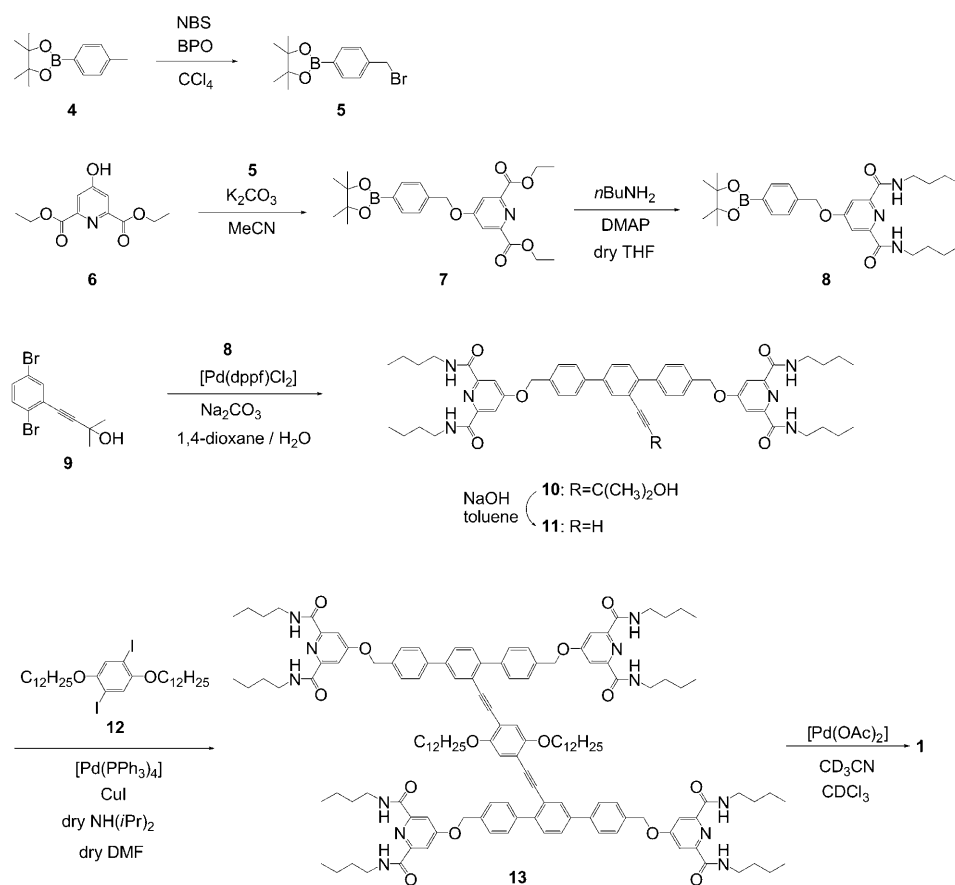
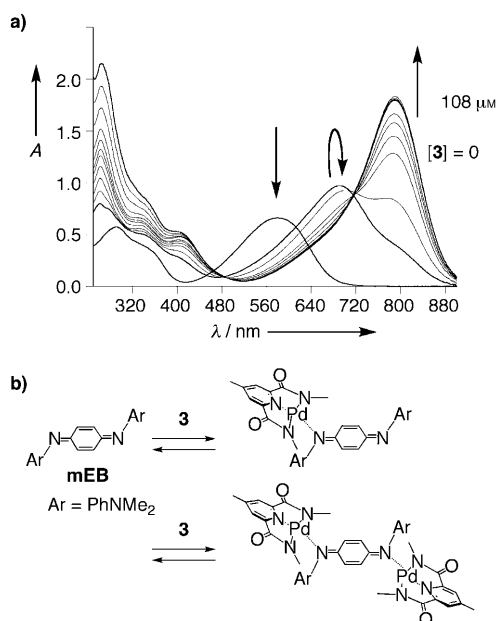
Molecular design and synthesis: The design of cross-linker (aligner) molecules is of importance to generate programmed assemblies of conjugated polymers with defined spacings and arrangements. We have recently utilized the dative bonds between porphyrinatozinc and diamine moiety in PPE to cross-link PPEs, which contribute to the high affinity and distinct bonding geometry. To design an aligner molecule for cross-linking **EB** and **ES**, we chose a palladium complex similar to that developed by Hirao et al.,^[15,16] because we expected high affinity toward the imine moiety in **EB**. We thus designed an aligner molecule **1** bearing two palladium tweezers, each of which consists of two palladium centers. The palladium-complex-based binding sites in **1** can freely rotate around the phenylene-1,4-diyne axle, whereas the rotation is suppressed when the guest(s) binds to the clefts. In this process, the binding of the first guest molecule or polymer to an aligner molecule facilitates the second binding, which should result in the ready formation of aligned assemblies, as we previously reported (Scheme 1b).^[12,13] As a result, each pair of the palladium complexes in **1** cross-links diimine moiety of **EB** and **ES** in an allosteric manner to form polymer bundles. In such polymer bundles, the distance between the two binding subunits was estimated to be about 2.3 nm by computational methods (Insight II, Discover, see Supporting Information). Thus, compound **1** was synthesized according to Scheme 2, and identified by ¹H NMR, MALDI TOF MS spectroscopic evidence and elemental analysis. Compounds **2** and **3** were synthesized and used for control experiments (Scheme S1 in the Supporting Information).



Scheme 1. a) Chemical structures of aligner, control molecules and conjugated polymers used in this study. b) Schematic illustration of the alignment of polyaniline (**EB**) by **1**. The first polymer binding event to **1** predisposes the second recognition site (denoted by the asterisk) such that it has an even higher affinity toward the second polymer. **EB**s are expected to be bundled to each other to form organized assemblies.

Complexation behavior of a repeating unit analogue, **mEB**:

We first used a low-molecular-weight and a repeating unit analogue of **EB** (thereafter, **mEB**) so as to confirm the complexation behaviors between imine moieties and **1** and **3**. Upon addition of **3** to a solution of **mEB** in THF, absorption maxima of **mEB** shifted from 580.0 to 686.0, then to 790.0 nm with two distinct isosbestic points (Figure 1a and Figure S2 in the Supporting Information). This stepwise complexation of **3** to **mEB** is rationalized by the view that two imine moieties were coordinated with palladium(II) in a sequential manner, as depicted in Figure 1b. Observed spectral changes are coincident with those observed for the study

Scheme 2. Synthetic scheme for the preparation of aligner molecule **1**.Figure 1. a) UV/Vis spectral changes of **mEB** ($27 \mu\text{M}$) upon addition of **3** (0 – $108 \mu\text{M}$) in THF at 25°C . b) Schematic illustration of complexation between **mEB** and **3**.

on the palladium-complex-**mEB** coordination system reported by Hirao et al.^[15]

Meanwhile, the **1·mEB** complex was formed in a cooperative manner. Formation of the complex was estimated from changes in the UV/Vis absorption spectra of **mEB** ($112 \mu\text{M}$) upon the successive addition of **1** (0 – $158 \mu\text{M}$) to a solution of **mEB** in THF (Figure 2a). The values of λ_{max} of **mEB** shifted to longer wavelengths from 581.0 to 790.0 nm with distinct isosbestic points (470.0 and 629.0 nm), indicating that the reaction between **mEB** and **1** consists of only two species under one equilibrium. From the plots of absorbance versus $[\mathbf{1}]/[\mathbf{mEB}]$ (Figure 2a inset), the stoichiometry between **1** was confirmed to be $1:2$ ($[\mathbf{1} \cdot (\mathbf{mEB})_2]$). It is worth noting that unlike conventional palladium complex **3**, the four palladium centers in **1** coordinate to imine moieties of two **mEB** molecules under equilibrium.

To obtain quantitative information, **1** ($5.9 \mu\text{M}$) was re-titrated with **mEB** (0 – $48 \mu\text{M}$) in THF at 25°C and followed by UV/Vis absorption spectroscopy (Figure S3 in the Supporting Information). The differential spectral changes enabled us to evaluate the complex formation of **1·mEB**; upon increasing **mEB** concentration, the absorption band of 367.0 nm of **1** shifted to a longer wavelength region (390.0 nm) with an isosbestic point (363.5 nm). Importantly, plots of absorbance at 390.0 nm versus $[\mathbf{mEB}]$ showed a sigmoidal curvature characteristic of positive homotropic allostery. These **mEB** bindings to **1** were initially analyzed with the Hill equation:^[17] $\log\{y/(1-y)\} = n_H \log[\text{guest}] + \log K$, in which K , y , and n_H are the association constant, extents of saturation, and Hill coefficient, respectively, and $y = K/([\text{guest}]^{-n} + K)$. From the slope and the intercept of the linear plots (Hill plot), we obtained $\log K$ and n_H (Figure S3 in the Supporting Information). The Hill coefficient n_H of 2.0 indicates that the **mEB** binding occurs cooperatively, since a higher value of n_H is related to a higher degree of cooperativity^[18] and the maximum is equal to the number of available binding subunits; in this case, **1** has two binding sites for **mEB**. From analysis of the binding isotherm in Figure 2c using a standard non-linear curve fitting method, we calculated the association constants (K_n [M^{-1}]) to be $K_1 = 2.2 \times 10^4$ and $K_2 = 9.4 \times 10^5$ for the formation of $\mathbf{1} \cdot (\mathbf{mEB})_2$. These results clearly show that the positive cooperative

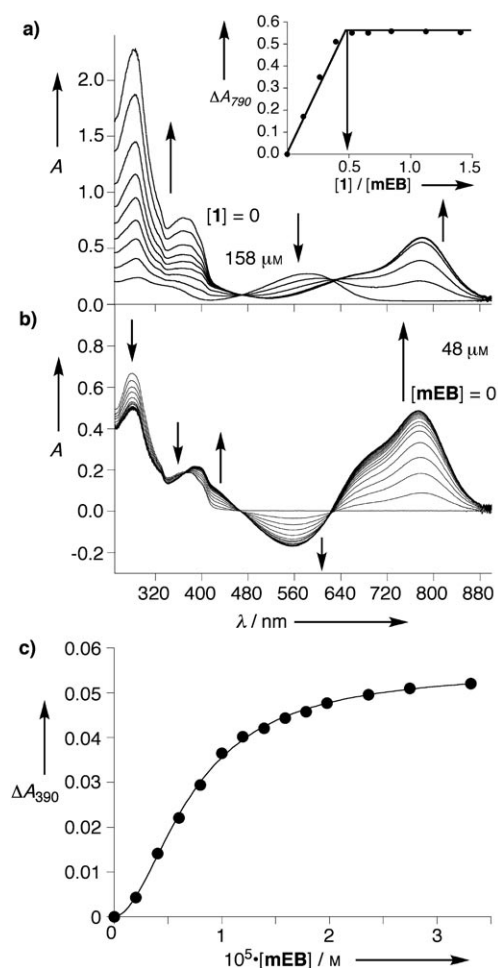
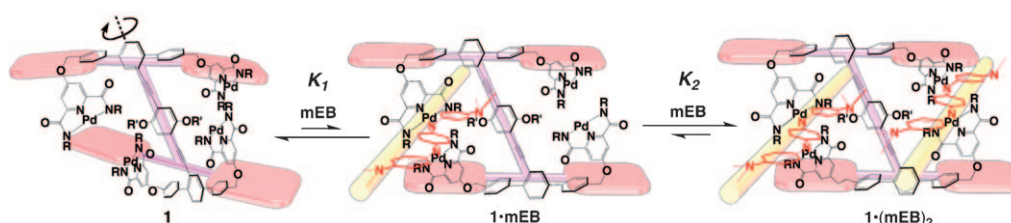


Figure 2. a) UV/Vis spectral changes of **mEB** (112 μM) upon addition of **1** (0–158 μM) in THF at 25 $^{\circ}\text{C}$. Inset: Plots of absorbance at 790.0 nm of **mEB** (112 μM) vs. $[\mathbf{1}]/[\mathbf{mEB}]$. b) Differential spectral changes of **1** ($[\mathbf{1}] = 5.9 \mu\text{M}$) upon addition of **mEB** ($[\mathbf{mEB}] = 0\text{--}48 \mu\text{M}$); this spectral changes were obtained by the subtraction of the absorption spectra of **mEB** from Figure S3a in the Supporting Information. c) Plots of the absorbance at 390.0 nm of **1** (5.9 μM) versus $[\mathbf{mEB}]$. The solid line represents the theoretical curve for the formation of 1:2 $[\mathbf{1}\cdot(\mathbf{mEB})_2]$ complex. We used solution of **1** in chloroform/acetonitrile (1:1) as a stock solution. Without acetonitrile, the palladium complexes of **1** tend to form oligomers via intermolecular coordination of carbonyl moieties to palladium complexes (see reference [16]).

binding takes place between **1** and **mEB**.^[19,20] This is because the binding of the first **mEB** moiety to one set of palladium



Scheme 3. Schematic representation for cooperative recognition process between **1** and **mEB**. The binding of the first **mEB** moiety to **1** suppresses the rotational motion of the phenylene-1,4-diyne axle in **1**, which facilitates the binding of the second **mEB** moiety. As a result, highly cooperative binding of **mEB** to **1** is achieved.

tweezers in **1** suppresses the motion around the phenylene-1,4-diyne axis in **1**,^[21] which facilitates the binding of the second **mEB** moiety, as illustrated in Scheme 3.

To obtain further insight into the $\mathbf{1}\cdot(\mathbf{mEB})_2$ complex, ^1H NMR spectra for $[\mathbf{1}]/[\mathbf{mEB}] = 1:0\text{--}1:2$ have been measured in $[\text{D}_1]\text{chloroform}/[\text{D}_3]\text{acetonitrile}$ 1:1 mixed solvent ($[\mathbf{1}] = 0.73 \text{ mM}$, Figure 3). The complexation-induced chemi-

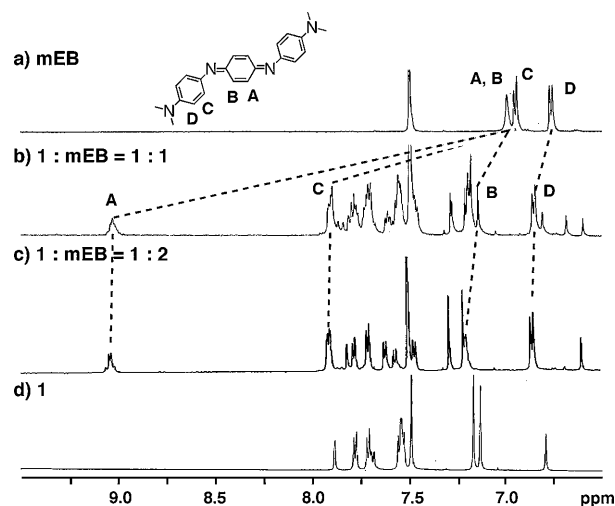


Figure 3. ^1H NMR spectra of a) **mEB** ($[\mathbf{mEB}] = 1.46 \text{ mM}$), b) $\mathbf{1}:\mathbf{mEB} = 1:1$ ($[\mathbf{1}] = [\mathbf{mEB}] = 0.73 \text{ mM}$), c) $\mathbf{1}:\mathbf{mEB} = 1:2$ ($[\mathbf{1}] = 0.73 \text{ mM}$, $[\mathbf{mEB}] = 1.46 \text{ mM}$), and d) **1** ($[\mathbf{1}] = 0.73 \text{ mM}$) in $[\text{D}_1]\text{chloroform}/[\text{D}_3]\text{acetonitrile}$ 1:1 mixed solvent at 298 K.

cal shifts of **mEB** protons gradually moved to a lower magnetic field up to $[\mathbf{1}]/[\mathbf{mEB}] = 1:2$ ratio and were then saturated. No peak broadening due to the formation of supramolecular polymer between **1** and **mEB** occurred in this system. It is known that **mEB** adopts two different conformations, *anti*- and *syn*-conformations in solution, although one cannot distinguish them by NMR spectroscopy due to the fast exchange at room temperature. The observed peaks for **mEB** complexed with **1** appear as four doublets that are assignable to *anti*-conformation. These results are consistent with those observed for the study on the palladium-complex-**mEB** coordination system.^[15a] We confirmed from these NMR and UV/Vis spectroscopic studies that the palladium complexes in **1** cooperatively recognize two **mEB** molecules in an *anti*-conformation (Scheme 3 and Figure 3). The

appearance of this high cooperativity in the binding of **mEB** and its complexation in an *anti*-conformation play a significant role for organizing **EB** into aligned, rather than random assemblies or ladder-type assemblies.^[22] In the polyaniline bundling process using **1**, the binding of the first **EB** moiety to **1** facilitates the binding of the second moiety, which results in the ready formation of aligned assemblies (Scheme 1 b).

Supramolecular assemblies of EB with 1–3: From the above-mentioned findings, one can expect that the diimine moieties in the repeating unit of **EB** would be recognized cooperatively in an *anti*-conformation by **1** and then become bundled, because the association constants are high enough. Indeed, the addition of **1** to a solution of **EB** ($M_n=20000$, $[\text{EB}]_{\text{unit}}=15\ \mu\text{M}$; $[\text{EB}]_{\text{unit}}$ denotes the concentration of the repeating unit of **EB** in Scheme 1 a) in THF at 25 °C resulted in the bathochromic shifts of λ_{max} of **EB** from 598.0 to 785.0 nm with broadening of the absorption band up to 1200 nm (Figure 4). This spectral change is similar to those

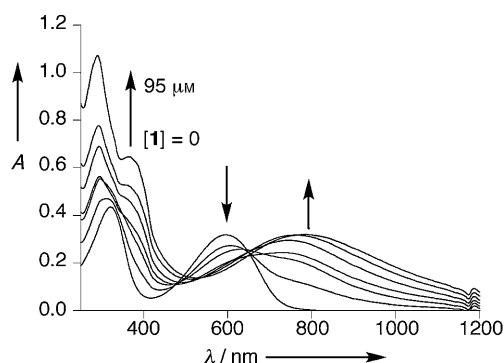


Figure 4. UV/Vis/NIR spectral changes of $[\text{EB}]_{\text{unit}}$ ($15\ \mu\text{M}$) upon addition of **1** (0–95 μM) in THF at 25 °C.

observed for **1·mEB** and those observed upon doping **EB** with protons (vide infra). These results indicate that diimine moieties of **EB** make coordination bonds with the palladium complexes in **1**. When we used longer **EB** ($M_n=300000$, $[\text{EB}]_{\text{unit}}=15\ \mu\text{M}$), a shift of λ_{max} from 602.0 to 778.0 nm was observed upon increase of the concentration of **1**. The poor solubility in THF of longer **EB** as well as its assembly with **1**, however, produced a bottleneck that limited the acquisition of further information.

The electron micrographs and electron diffraction patterns of **EB** assemblies provide information regarding how **EB** are organized into aligner·**EB** assemblies. Firstly, we prepared solution-cast films of **1**, **2**, or **EB** ($M_n=20000$) and confirmed using TEM that the aligner or **EB** alone is not able to make organized assemblies; only amorphous aggregates with the size of a few hundred by a few hundred nm were produced on the TEM grid (see Figure S4 and S5a in the Supporting Information). In cases in which **2** and **3** are used as the palladium complexes to form **EB** assemblies, we confirmed from TEM observation that amorphous assem-

blies are dominant (Figure S6 in the Supporting Information). This is because complex **3** cannot cross-link **EBs** and **2** cannot exhibit cooperativity in the binding of **EBs**. Only under the conditions in which the $[\text{2}]/[\text{EB}]_{\text{unit}}$ ratio was over 0.5, were partially crystalline **2·EB** assemblies obtained (Figure S6b in the Supporting Information).

We subjected the sample prepared from **EB** and **1** to TEM observation so as to reveal how **1·EB** assemblies are organized. We prepared solution-cast films of the **1·EB** assemblies formed in various mixing ratios of $[\text{1}]$ and $[\text{EB}]_{\text{unit}}$ on a TEM grid. Given the association constants we obtained in this study, complex **1** is supposed to complex completely with **EB** under the conditions we used. Among seven samples with $[\text{1}]/[\text{EB}]_{\text{unit}}=0:1-0.5:1$ mixing ratio, micron-sized sheet morphologies with clear electron diffraction patterns were observed under the conditions of $[\text{1}]/[\text{EB}]_{\text{unit}}=0.20:1$ to $0.25:1$ (Figure S5 and S7 in the Supporting Information). This higher cross-linking ratio than that found in our previous supramolecular organization of poly(phenyleneethynylene)s bearing alkyl chains is probably due to the lack of alkyl chains in **EB**. To maintain sheet morphologies with the periodicity of nm scale, we infer that alkyl chains in the polymer and/or aligner are of importance. In the image of a thick assembly prepared with the mixing ratio of $[\text{1}]/[\text{EB}]_{\text{unit}}=0.20:1$, we observed a crossed dark stripe contrast together with moiré fringes (Figure 5 a and 5 b), indicating that a few thin sheets with striped structures were overlapped and the alignment among sheet assemblies could not be achieved in this system. Figure 5 c displays HRTEM images of the **1·EB** assemblies ($[\text{1}]/[\text{EB}]_{\text{unit}}=0.20:1$) in which the periodicity of the multilamellar contrast, over a distance of a few hundred nanometers, was 2.5 nm, as determined from the Fourier-filtered image. Judging from data reported previously,^[12,13] we deduce that the darker sections in the electron micrographs of **1·EB** assemblies are domains containing ordered π -stacked layers and Pd (the heaviest atom). Indeed, the energy dispersive X-ray spectroscopic (EDX) study on the **1·EB** assembly revealed that the sheet structure contains Pd (Figure S7 in the Supporting Information), although from EDX analysis we could not specify spatial distribution of Pd. As mentioned above, Pd^{II} atoms coordinate to the imine moieties in **EB** and, therefore, the **EB** are probably ordered along these dark contrast regions. It is worth noting that the distance of 2.5 nm is almost identical to that which we calculated when **EBs** are bundled by **1** in an *anti*-conformation.

Pre-doping before adding aligner molecule: We tried to pre-dope **EB** before complexation with **1**, because the acidity of $\text{EB}\cdot\text{nH}^+$ (emeraldine salt: **ES**) is much lower than that of commonly used dopant acids such as sulfonic acids. The protons in **ES** could be displaced by the palladium centers in **1** to produce the **1·ES** assembly (Scheme 4). The in situ addition of camphor sulfonic acid (CSA) to a solution of **EB** in THF,^[23] which should induce protonation of the imine groups in **EB** to produce **ES** units, was monitored by UV/Vis/NIR absorption spectral methods. The λ_{max} of **ES** ap-

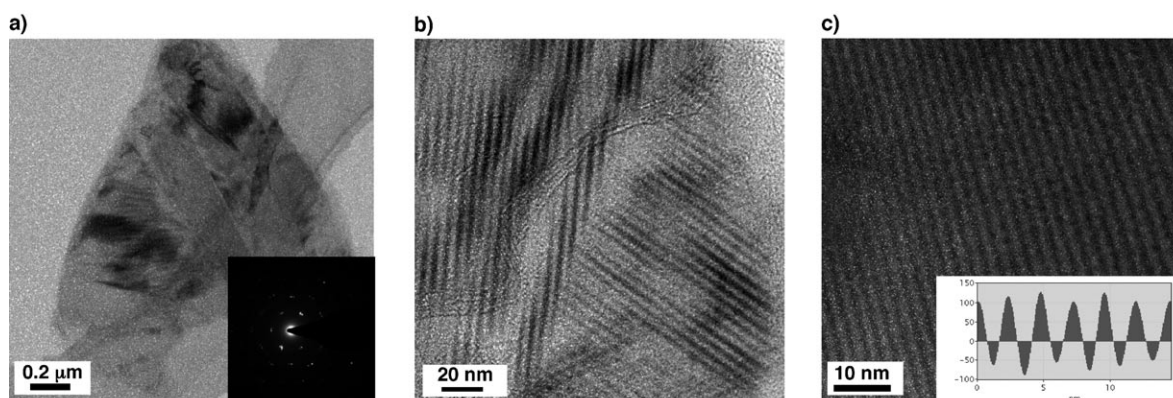
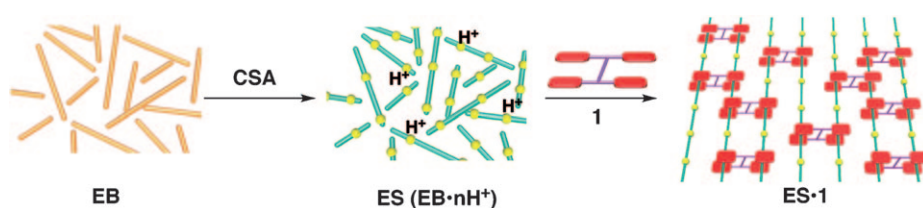


Figure 5. Electron micrographs (no staining) of **EB** aligned by **1**. a) TEM image of **1-EB** assemblies. ($[\text{EB}]_{\text{unit}} = 12 \mu\text{M}$ and $[\text{1}] = 2.4 \mu\text{M}$) Inset: Electron diffraction pattern. b) Enlarged view of a). c) HRTEM images of **1-EB** assemblies consisting of alternating dark and light stripes and extracted perodpocal patterns from Fourier translation image. The periodicity between dark lines is 2.5 nm.



Scheme 4. Schematic illustration of the formation of **1-ES** assembly.

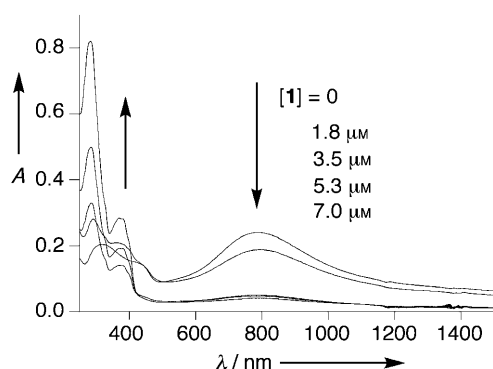


Figure 6. UV/Vis/NIR spectral changes of **ES** ($[\text{ES}]_{\text{unit}} = 14 \mu\text{M}$) upon addition of **1** (0–7.0 μM) in THF at 25 °C. High substitution ratio of **1** (over $[\text{1}]/[\text{ES}]_{\text{unit}} = 0.125:1$) resulted in the decrease of absorbance of **ES** due to the precipitation.

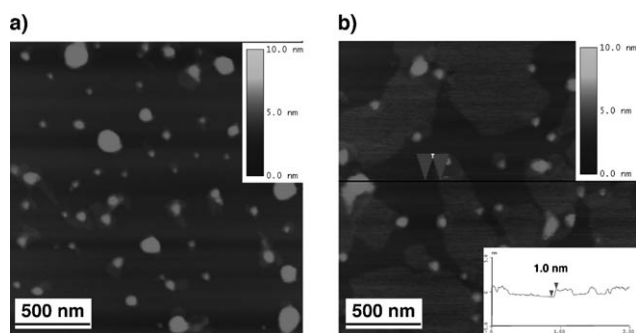


Figure 7. AFM images of a) **ES** assembly and b) **1-ES** assembly ($[\text{1}]/[\text{ES}]_{\text{unit}} = 0.125:1$, $[\text{ES}]_{\text{unit}} = 1.5 \mu\text{M}$). Inset: the height profile of the black line in a).

peared at 782.0 nm with broadening of the absorption band up to 1200 nm; the characteristic polaron absorption^[23] appeared at 435.0 nm. Upon addition of **1** to a solution of **ES** in THF, partial displacement from protons in **ES** to the palladium centers of **1** was observed.

A high substitution ratio of **1** (over $[\text{1}]/[\text{ES}]_{\text{unit}} = 0.250:1$), however, resulted in precipitation of **1-ES** assembly (over ten micron-sized sheet assemblies) and entangled **1-ES** assemblies (granular assemblies) were observed in the TEM images (Figure S8 in the Supporting Information). Under the conditions of $[\text{1}]/[\text{ES}]_{\text{unit}} = 0.125:1$, the shift of absorption maxima of **ES** from 782.0 to 793.0 nm indicates that a displacement reaction occurred (Figure 6). We further confirmed the formation of **1-ES** assemblies by using atomic force microscopy (AFM), TEM and HRTEM (Figures 7 and 8).

Figure 7a displays an AFM image of **ES** (deposited from a 1.5 μM solution in THF) in which **ES** assembly is dispersed in a dot shape^[24] on HOPG; by mixing **ES** ($[\text{ES}]_{\text{unit}} = 1.5 \mu\text{M}$) with **1** (0.18 μM) in solution, large sheet morphologies with a height of 1.0 nm were observed (Figure 7b). Given the degree of polymerization of **ES**, **1** must bundle with and noncovalently splice **ES** to form such supramolecular **1-ES** assemblies. It is shown from TEM and HRTEM images in Figure 8 (and Figure S8 in the Supporting Information) that crystalline sheet morphologies with multilamellar contrast were dominant. Furthermore, EDX studies clearly showed that the crystalline sheet morphologies contain Pd together with sulfur, which comes from dopant CSA. The stripe periodicity of 2.5 nm over a 200 nm-wide distance in the multilamellar contrast was determined from the Fourier-filtered image (Figure 8b). The distance of 2.5 nm is identical to that observed for **1-EB** assemblies, indicating that **ES**s are bundled by **1** in an *anti*-conformation to yield the crystalline assemblies. Most likely the interpolymer spacing of 2.5 nm

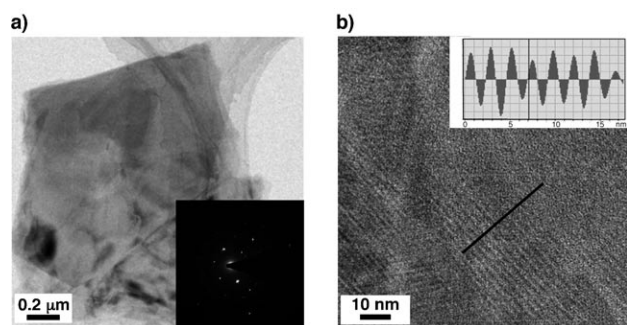


Figure 8. Electron micrographs (no staining) of **ES** aligned by **1**. a) TEM images of **1-ES** assemblies ($[\text{ES}]_{\text{unit}} = 14 \mu\text{M}$, $[\text{1}]/[\text{ES}]_{\text{unit}} = 0.125:1$). Inset: Electron diffraction pattern of a), indicating that the assemblies show the crystalline nature. b) HRTEM images of **1-ES** assemblies consisting of alternating dark and light stripes and extracted periodical patterns from Fourier translation image. The periodicity between dark lines is 2.5 nm.

would be large enough to accept dopant CSAs within **1-ES** assemblies.

The electric conductivity of the samples was measured by using a four-point probe. We first tried to measure a thin film prepared by means of spin coating; however, we could not obtain reliable values. We thus prepared solution-cast films of **ES** ($[\text{ES}]_{\text{unit}} = 240 \mu\text{M}$) and **1-ES** assemblies ($[\text{ES}]_{\text{unit}} = 240 \mu\text{M}$, $[\text{1}]/[\text{ES}]_{\text{unit}} = 0.125:1$) formed in THF on a glass plate. The bulk conductivity was calculated from surface resistivity and film thickness. The conductivity of 0.19 Scm^{-1} for **1-ES** assemblies is the same as that of **ES** (0.20 Scm^{-1}). We infer that the aligner molecule **1** acts as a charge carrier trap.^[25] Moreover, the alignment of sheet assemblies could not be achieved in this system, as indicated by our TEM measurements. These could be the reasons why the conductivity of **1-ES** assemblies is not so high in comparison with that of **ES** and thereby, the effect of the alignment of **ES**s by the aid of **1** would be canceled out.

Conclusions

Since the discovery of conducting polymers, it has been the goal of many research efforts to control the molecular orientation and alignment of these materials, especially because the molecular alignment appears to be important in increasing conductivity. The supramolecular bundling approach inspired by the mode of action of actin filament bundling proteins is now applicable to polyanilines (**EB** and **ES**) to organize into crystalline assemblies. We designed and synthesized aligner **1**, bearing four Pd centers, which exhibited high cooperativity and high affinity in the binding of two **mEB**s. Furthermore, use of **1** enabled us to monitor the binding process of **mEB**, **EB**, and **ES** by means of UV/Vis, UV/Vis/NIR, NMR spectroscopy, and electron microscopes in order to analyze their crystalline assemblies. The results obtained so far showed that the palladium coordination to the imine moieties in **EB** and **ES** results in the formation of crystalline assemblies with the periodicity of 2.5 nm, which

is determined by the distance between binding sites in **1**. Compound **1** could act as a carrier trap that hampers the higher conduction. We deduce, however, that the decrease in conductivity by the palladium binding is minimal because the effect of alignment of **ES** by **1** would have an antagonistic activity towards the decrease in the conductivity. Basically, this approach would resolve two critical issues associated with conjugated polymer-based devices; the segregation of polymers in individual chains and controlled alignment. Introducing new interaction sites toward **EB** and **ES**, such as sulfonic acid based binding sites for imines, would result in the formation of crystalline assemblies expected to have higher conductivity. Furthermore, by introducing liquid-crystalline moieties into aligner molecules, the alignment of sheet assemblies would be achieved.

Experimental Section

General: All starting materials and solvents were purchased from Aldrich, Tokyo Kasei Chemicals or Wako Chemicals and used as received. The ^1H NMR spectra were recorded on a Bruker DRX 600 (600 MHz) spectrometer. **EB**s were purchased from Aldrich and used without purification. Chemical shifts are reported in ppm downfield from tetramethylsilane as the internal standard. Mass spectral data were obtained using a Perceptive Voyager RP MALDI TOF mass spectrometer, a JEOL JMS HX110 A high-resolution magnetic sector FAB mass spectrometer, Bruker micrOTOF focus high-resolution CSI mass spectrometer, and a JEOL JMS T100CS high-resolution ESI mass spectrometer. UV/Vis and UV/Vis/NIR spectra were recorded using Shimadzu UV-2500 PC and UV-3100 spectrophotometer, respectively.

Binding isotherm analysis: The cooperative guest-binding process was analyzed according to the Hill equation: $\log\{y/(y-1)\} = n_{\text{H}} \log[\text{guest}] + \log K$, in which K , y , and n_{H} are the association constant, the extent of complexation, and the Hill coefficient, respectively. The slope and the intercept of the linear (Hill) plots allow K and n_{H} to be estimated; these values are useful measures of cooperativity. A higher value of n_{H} is related to a higher degree of cooperation; the maximum value is equal to the number of binding sites. In the analysis of binding isotherm from the Hill plot, we evaluated the concentration of unbound guest ($[\text{guest}]$) by assuming that the 1:2 complex of **1** is formed quantitatively when the absorption change is saturated.

Transmission electron microscopy (TEM), high-resolution TEM (HRTEM), and atomic force microscopy (AFM) measurements: TEM and HRTEM images were acquired using a JEOL TEM-2010 (accelerating voltage: 120 kV) and a TECNAI-20 FEI (accelerating voltage: 200 kV), respectively. A sample solution was placed on a copper TEM grid upon a holey carbon support film. Energy dispersive spectroscopy (EDX) spectra and EDX line scan profiles were obtained using a TECNAI-20, FEI. The TEM grid was dried under reduced pressure for 6 h prior to TEM observation. AFM images were acquired in air using a NanoScope IIIa (tapping mode).

Sample preparation for TEM and AFM measurements: A solution of the sample in THF was cast on a copper TEM grid upon a holey carbon support film. The sample was prepared by drop casting on HOPG and dried for 6 h under reduced pressure before TEM and AFM observation.

Conductivity measurements: The conductivity of the samples ($[\text{EB}]_{\text{unit}} = 240 \mu\text{M}$) was measured using a four-point probe (1116SLD, BAS Inc.). The probe was equipped with four spring-loaded tungsten carbide needles spaced 1 mm apart. The conductivity of the **EB-CSA (ES)** and **EB-CSA-1** film coated on the glass plate was calculated from the surface resistivity and the film thickness, which was measured by an α -step surface procedure.

Synthesis: Compounds used in this study were synthesized according to Scheme 2 and Scheme S1 in the Supporting Information. Compound **4** was purchased and used without further purification. Compounds **6**,^[26] **9**,^[27] and **12**^[12] were synthesized according to the method in the literature.

2-(4-Bromomethylphenyl)-4,4,5,5-tetramethyl-1,3,2-dioxaborolane (5): In a 300 mL round-bottomed flask, benzoyl peroxide (BPO; 0.27 g, 1.1 mmol, 0.05 equiv) was added to a solution of **4** (4.8 g, 22 mmol, 1 equiv) and *N*-bromosuccinimide (NBS; 4.3 g, 24 mmol, 1.1 equiv) in tetrachloromethane (150 mL) under an N₂ atmosphere. The reaction mixture was kept under reflux for 3 h. The reaction was monitored by TLC (silica gel, chloroform: *n*-hexane = 1:2 (v/v)). After completion, the insoluble materials were filtered off and the filtrate was evaporated. Compound **5** was isolated as a white solid (4.6 g, 71 %) by recrystallization from ethanol. ¹H NMR (600 MHz, CDCl₃, TMS standard, RT): δ = 1.34 (s, 12H), 4.49 (s, 2H), 7.39 (d, *J* = 7.9 Hz, 2H), 7.78 ppm (d, *J* = 7.9 Hz, 2H); elemental analysis calcd (%) for C₁₃H₁₈BBrO₂: C 52.57, H 6.11; found: C 52.82, H 5.95.

Diethyl 4-[4-(4,4,5,5-tetramethyl-1,3,2-dioxaborolan-2-yl)benzyloxy]pyridine-2,6-dicarboxylate (7): In a 200 mL round-bottomed flask, **5** (2.5 g, 8.4 mmol, 1.1 equiv) was added to a solution of K₂CO₃ (2.2 g, 16 mmol, 2.0 equiv) and **6** (1.9 g, 8.0 mmol, 1 equiv) in dry acetonitrile (50 mL). The solution was stirred at 85 °C for 2.5 h. The reaction was monitored by TLC (silica gel, dichloromethane). After completion, the insoluble materials were filtered off and the filtrate was evaporated. Diethyl ether was added to the residue and the resulting solution was washed with H₂O and dried over anhydrous Na₂SO₄. The residue was purified by column chromatography (silica gel, chloroform/methanol 10:1) to produce **7** as a white solid (2.5 g, 69 %). ¹H NMR (600 MHz, CDCl₃, TMS standard, RT): δ = 1.35 (s, 12H, s), 1.41 (t, *J* = 6.9 Hz, 6H), 4.47 (q, *J* = 7.2 Hz, 4H), 5.24 (s, 2H), 7.43 (d, *J* = 7.7 Hz, 2H), 7.85–7.86 ppm (m, 4H); MALDI TOF MS (dithranol): *m/z* calcd for [M+H]⁺ = 456.21; found: 455.9853; elemental analysis calcd (%) for C₂₄H₃₀BNO₇: C 63.31, H 6.64, N 3.08; found: C 63.17, H 6.67, N 3.12.

4-(4-(4,4,5,5-Tetramethyl-1,3,2-dioxaborolan-2-yl)benzyloxy)-*N,N*-dibutylpyridine-2,6-dicarboxamide (8): In a 300 mL round-bottomed flask, *n*-butylamine (27 mL, excess) was added to a solution of **7** (1.0 g, 2.2 mmol, 1 equiv) and DMAP (530 mg, 4.4 mmol, 2 equiv) in dry THF (40 mL). The reaction was kept under reflux for 68 h under Ar atmosphere. The reaction was monitored by TLC (silica gel, chloroform/methanol 10:1). The solvent was evaporated. Chloroform was added to the residue and the resulting solution was washed by H₂O (50 mL × 3) and dried over anhydrous Na₂SO₄. The insoluble materials were filtered off, and the filtrate was purified by column chromatography (silica gel, chloroform/methanol 10:1) to produce **8** as a white solid (1.0 g, 91 %). ¹H NMR (600 MHz, CDCl₃, TMS standard, RT): δ = 0.98 (t, *J* = 7.3 Hz, 6H), 1.34 (s, 12H), 1.41–1.47 (m, 4H), 1.62–1.67 (m, 4H), 3.50 (q, *J* = 6.9 Hz, 4H), 5.25 (s, 2H), 7.42 (d, *J* = 7.9 Hz, 2H), 7.65 (s, 2H), 7.83 (d, *J* = 7.9 Hz, 2H), 7.90 ppm (s, 2H); MALDI TOF MS (dithranol): *m/z* calcd for [M+H]⁺: 510.31; found: 509.9092; HR FABMS: *m/z* calcd for [M+H]⁺: 510.3061; found: 510.3112; elemental analysis calcd (%) for C₂₈H₄₀BN₃O₅: C 66.01, H 7.91, N 8.25; found: C 65.99, H 7.91, N 8.24.

Compound 10: In a 100 mL two-neck flask, an aqueous solution of Na₂CO₃ (9 mL; 290 mg, 2.8 mmol, 3 equiv) and [Pd(dppf)Cl₂] (150 mg, 0.18 mmol, 0.2 equiv) were added to a solution of **9** (290 mg, 0.92 mmol, 1 equiv) and **8** (1.4 g, 2.8 mmol, 3.0 equiv) in 1,4-dioxane (50 mL). The reaction was kept under reflux for 1.5 h under an Ar atmosphere. The reaction was monitored by TLC (silica gel, chloroform/methanol 30:1). After completion, the insoluble materials were filtered off and the filtrate was evaporated. The residue was washed with methanol and was then purified by column chromatography (silica gel, chloroform/acetonitrile 30:1) to produce **10** as a gray solid (580 mg, 69 %). ¹H NMR (600 MHz, CDCl₃, TMS standard, RT): δ = 0.97–1.00 (m, 12H), 1.43–1.47 (m, 8H), 1.50 (s, 6H), 1.63–1.68 (m, 8H), 2.30 (s, 1H), 3.49–3.53 (q, *J* = 6.9 Hz, 8H), 5.29–5.33 (m, 4H), 7.46 (d, *J* = 8.1 Hz, 1H), 7.49 (d, *J* = 8.0 Hz, 2H), 7.52 (d, *J* = 8.0 Hz, 2H), 7.60 (dd, *J* = 1.4, 8.9 Hz, 1H), 7.65–7.69 (m, 8H), 7.77 (d, *J* = 1.8 Hz, 1H), 7.93 (s, 2H), 7.95 ppm (s, 2H); MALDI TOF MS (dithranol): *m/z* calcd for [M+Na]⁺: 945.50; found: 945.5026; HR ESI TOF MS: *m/z* calcd for [M+H]⁺: 923.5071; found 923.5047.

Compound 11: In a 50 mL two-neck flask, NaOH (10 mg, excess) was added to a solution of **10** (20 mg, 22 μmol) in anhydrous toluene (6 mL). The reaction was kept under reflux for 5.5 h. The reaction was monitored by TLC (silica gel, chloroform/methanol 10:1). After completion, the insoluble materials were filtered off. The filtrate was evaporated to produce **11** as a slightly yellow solid (15 mg, 80 %). ¹H NMR (600 MHz, CDCl₃, TMS standard, RT): δ = 0.96–0.99 (m, 12H), 1.43–1.47 (m, 8H), 1.63–1.68 (m, 8H), 3.10 (s, 1H), 3.49–3.53 (m, 8H), 5.28 (s, 4H), 7.45 (d, *J* = 8.0 Hz, 1H), 7.51 (d, *J* = 8.7 Hz, 2H), 7.52 (d, *J* = 8.8 Hz, 2H), 7.63 (dd, *J* = 1.7, 8.1 Hz, 1H), 7.66 (d, *J* = 8.2 Hz, 2H), 7.68 (d, *J* = 8.2 Hz, 2H), 7.71 (s, 4H), 7.86 (d, *J* = 1.4 Hz, 1H), 7.95 (s, 2H), 7.96 ppm (s, 2H); MALDI TOF MS: *m/z* calcd for [M+H]⁺: 865.46; found: 865.3655; HR FABMS: *m/z* calcd for [M+H]⁺: 865.4574; found 865.4656.

Compound 13: In a 50 mL two-neck flask, anhydrous diisopropylamine (6.0 mL, excess) was added to a solution of **11** (190 mg, 0.22 mmol, 2.2 equiv), **12** (70 mg, 0.10 mmol, 1 equiv), [Pd(PPh₃)₄] (46 mg, 0.04 mmol, 0.4 equiv), and CuI (7.6 mg, 0.04 mmol, 0.4 equiv) in anhydrous DMF (14.0 mL). The reaction was stirred at 60 °C for 4.5 h under an Ar atmosphere. The solvent was evaporated and then chloroform was added to the residue. The solution was washed by saturated NH₄Cl solution (30 mL × 3) and H₂O (30 mL), then dried over anhydrous Na₂SO₄. The insoluble materials were filtered off and the filtrate was evaporated. The residue was purified by column chromatography (silica gel, chloroform/acetonitrile 10:1) to produce **13** as a yellow solid (57 mg, 26 %). ¹H NMR (600 MHz, CDCl₃, TMS standard, RT): δ = 0.82 (t, *J* = 7.2 Hz, 6H), 0.94–1.00 (m, 24H), 1.12–1.15 (m, 28H), 1.35–1.40 (m, 4H), 1.41–1.48 (m, 20H), 1.63–1.69 (m, 20H), 3.46–3.53 (m, 16H), 3.90 (t, *J* = 6.4 Hz, 4H), 5.25 (s, 4H), 5.29 (s, 4H), 6.77 (s, 2H), 7.49–7.54 (m, 10H), 7.61–7.63 (m, 2H), 7.68–7.72 (m, 8H), 7.79 (d, *J* = 8.0 Hz, 4H), 7.89–7.91 (m, 6H), 7.96 ppm (s, 8H); MALDI TOF MS (dithranol): *m/z* calcd for [M+H]⁺: 2195.30; found: 2195.2979.

Compound 1: Compound **1** was prepared according to the previously reported method.^[28] In a 25 mL two-neck flask, [Pd^{II}(OAc)₂] (17 mg, 74 μmol, 4.0 equiv) was added to a solution of **13** (40 mg, 18 mmol, 1 equiv) in acetonitrile (8.0 mL) and chloroform (4.0 mL) under an Ar atmosphere. The solution was stirred at room temperature for 1 day. The reaction was monitored by TLC (silica gel, chloroform/methanol 10:1). After completion, the insoluble materials were filtered off and the filtrate was evaporated to produce **1** as a yellow solid (46 mg, 90 %). ¹H NMR (600 MHz, [D₁]CDCl₃/[D₃]CD₃CN 1:1, TMS standard, RT): δ = 0.83 (t, *J* = 7.2 Hz, 6H), 0.95 (q, *J* = 7.2 Hz, 24H), 1.11–1.15 (m, 28H), 1.37–1.41 (m, 24H), 1.51–1.53 (m, 20H), 3.24 (q, *J* = 8.4 Hz, 16H), 3.94 (t, *J* = 6.2 Hz, 4H), 5.31 (s, 8H), 6.81 (s, 2H), 7.16 (s, 4H), 7.19 (s, 4H), 7.54–7.57 (m, 10H), 7.70 (dd, *J* = 1.5, 8.2 Hz, 2H), 7.72 (d, *J* = 8.1 Hz, 4H), 7.79 (d, *J* = 7.9 Hz, 4H), 7.89 ppm (d, *J* = 1.3 Hz, 2H); HR CSI TOF MS: *m/z* calcd for [(M+2Na)/2]²⁺: 1399.9698; found: 1399.9645.

Acknowledgements

M.T. and T.K. thank Dr. K. Sugiyasu of NIMS for valuable comments and Mr. M. Frank for reading of the manuscript. This study was supported partially by a Grant-in-Aid for Science Research in a Priority Area “Super-Hierarchical Structures” (19022026 to M.T.) and a Grant-in-Aid for Scientific Research for Priority Area Coordination Programming (area 2107) (21108010 to M.T.) from the Ministry of Education, Culture, Science, Sports, and Technology (Japan). T.K. thanks JSPS for the Research Fellowship for Young Scientists for financial support.

- [1] For reviews of conducting polymers, see: a) A. G. MacDiarmid, *Rev. Mod. Phys.* **2001**, *73*, 701–712; b) A. Pron, P. Rannou, *Prog. Polym. Sci.* **2002**, *27*, 135–190; c) A. G. MacDiarmid, *Angew. Chem.* **2001**, *113*, 2649–2659; *Angew. Chem. Int. Ed.* **2001**, *40*, 2581–2590; d) T. A. Skotheim, R. L. Elsenbaumer, J. R. Reynolds, *Handbook of Conducting Polymers*, 3rd ed., CRC Press, New York, **2007**.

- [2] a) F. Marchioni, J. Yang, W. Walker, F. Wudl, *J. Phys. Chem. B* **2006**, *110*, 22202–22206; b) F. Cheng, W. Tang, C. Li, J. Chen, H. Liu, P. Shen, S. Dou, *Chem. Eur. J.* **2006**, *12*, 3082–3088.
- [3] a) N. Stutzmann, R. H. Friend, H. Sirringhaus, *Science* **2003**, *299*, 1881–1884; b) R. J. Kline, M. D. McGehee, M. F. Toney, *Nat. Mater.* **2006**, *5*, 222–228; c) Z. Q. Li, G. M. Wang, N. Sai, D. Moses, M. C. Martin, M. D. Ventra, A. J. Heeger, D. N. Basov, *Nano Lett.* **2006**, *6*, 224–228.
- [4] a) R. H. Friend, R. W. Gymer, A. B. Holmes, J. H. Burroughes, R. N. Marks, C. Taliani, D. D. C. Bradley, D. A. Dos Santos, J. L. Brédas, M. Lögdlund, W. R. Salaneck, *Nature* **1999**, *397*, 121–128; b) A. P. Kulkarni, C. J. Tonzola, A. Babel, S. A. Jenekhe, *Chem. Mater.* **2004**, *16*, 4556–4573.
- [5] a) S. Günes, H. Neugebauer, N. S. Sariciftci, *Chem. Rev.* **2007**, *107*, 1324–1338; b) J. Peet, J. Y. Kim, N. E. Coates, W. L. Ma, D. Moses, A. J. Heeger, G. C. Bazan, *Nat. Mater.* **2007**, *6*, 497–500; c) M. Campoy-Quiles, T. Ferenczi, T. Agostinelli, P. G. Etchegoin, Y. Kim, T. D. Anthopoulos, P. N. Stavrinou, D. D. C. Bradley, J. Nelson, *Nat. Mater.* **2008**, *7*, 158–164.
- [6] For recent reports of polyaniline, see: a) K. Lee, S. Cho, S. H. Park, A. J. Heeger, C.-W. Lee, S.-H. Lee, *Nature* **2006**, *441*, 65–68; b) A. Aoki, R. Umehara, K. Banba, *Langmuir* **2009**, *25*, 1169–1174.
- [7] For polyaniline materials, see: a) G. Gustafsson, Y. Gao, G. M. Treacy, F. Klavetter, N. Colaneri, A. J. Heeger, *Nature* **1992**, *357*, 477–479; b) N. J. Pinto, A. T. Johnson, Jr., A. G. MacDiarmid, C. H. Mueller, N. Theofylaktos, D. C. Robinson, F. A. Miranda, *Appl. Phys. Lett.* **2003**, *83*, 4244–4246; c) S. Tan, J. Zhai, B. Xue, M. Wan, Q. Meng, Y. Li, L. Jiang, D. Zhu, *Langmuir* **2004**, *20*, 2934–2937; d) K. S. Lee, T. J. Smith, K. C. Dickey, J. E. Yoo, K. J. Stevenson, Y. L. Loo, *Adv. Funct. Mater.* **2006**, *16*, 2409–2414; e) M. Irimia-Vladu, N. Marjanovic, A. Vlad, A. M. Ramil, G. Hernandez-Sosa, R. Schwödiauer, S. Bauer, N. S. Sariciftci, *Adv. Mater.* **2008**, *20*, 3887–3892.
- [8] a) S. J. Su, M. Takeishi, N. Kuramoto, *Macromolecules* **2002**, *35*, 5752–5757; b) Y. Yan, K. Deng, Z. Yu, Z. Wei, *Angew. Chem.* **2009**, *121*, 2037–2040; *Angew. Chem. Int. Ed.* **2009**, *48*, 2003–2006; c) B. A. Deore, M. S. Freund, *Macromolecules* **2009**, *42*, 164–168.
- [9] a) H. Kosonen, J. Ruokolainen, M. Knaapila, M. Torkkeli, K. Jokela, R. Serimaa, G. ten Brinke, W. Bras, A. P. Monkman, O. Ikkala, *Macromolecules* **2000**, *33*, 8671–8675; b) Z. Wei, T. Laitinen, B. Smarsly, O. Ikkala, C. F. J. Fault, *Angew. Chem.* **2005**, *117*, 761–766; *Angew. Chem. Int. Ed.* **2005**, *44*, 751–756; c) M. Vilkmann, H. Kosonen, A. Nykanen, J. Ruokolainen, M. Torkkeli, R. Serimaa, O. Ikkala, *Macromolecules* **2005**, *38*, 7793–7797.
- [10] a) K. Yoshida, T. Shimomura, K. Ito, R. Hayakawa, *Langmuir* **1999**, *15*, 910–913; b) M. Numata, T. Hasegawa, T. Fujisawa, K. Sakurai, S. Shinkai, *Org. Lett.* **2004**, *6*, 4447–4450; c) Y. Liu, J. Shi, Y. Chen, C.-F. Ke, *Angew. Chem.* **2008**, *120*, 7403–7406; *Angew. Chem. Int. Ed.* **2008**, *47*, 7293–7296.
- [11] a) A. P. Monkman, P. Adams, *Synth. Met.* **1991**, *40*, 87–96; b) P. Quint, W. Knoll, M. Hara, H. Sasabe, R. S. Duran, *Macromolecules* **1995**, *28*, 4029–4032; c) J. Y. Josefowicz, J. K. Avlyanov, A. G. MacDiarmid, *Thin Solid Films* **2001**, *393*, 186–192; d) B. Dufour, P. Rannou, P. Fedorko, D. Djurado, J. P. Travers, A. Pron, *Chem. Mater.* **2001**, *13*, 4032–4040; e) O. P. Dimitriev, *J. Colloid Interface Sci.* **2003**, *262*, 574–578; f) A. D. W. Carswell, E. A. O'Rear, B. P. Grady, *J. Am. Chem. Soc.* **2003**, *125*, 14793–14800; g) L. Y. O. Yang, C. Chang, S. Liu, C. Wu, S. L. Yau, *J. Am. Chem. Soc.* **2007**, *129*, 8076–8077.
- [12] a) Y. Kubo, Y. Kitada, R. Wakabayashi, T. Kishida, M. Ayabe, K. Kaneko, M. Takeuchi, S. Shinkai, *Angew. Chem.* **2006**, *118*, 1578–1583; *Angew. Chem. Int. Ed.* **2006**, *45*, 1548–1553; b) R. Wakabayashi, Y. Kubo, K. Kaneko, M. Takeuchi, S. Shinkai, *J. Am. Chem. Soc.* **2006**, *128*, 8744–8745; c) R. Wakabayashi, K. Kaneko, M. Takeuchi, S. Shinkai, *New J. Chem.* **2007**, *31*, 790–799.
- [13] M. Takeuchi, C. Fujikoshi, Y. Kubo, K. Kaneko, S. Shinkai, *Angew. Chem.* **2006**, *118*, 5620–5625; *Angew. Chem. Int. Ed.* **2006**, *45*, 5494–5499.
- [14] J. Sakamoto, J. van Heijst, O. Lukin, A. D. Schlüter, *Angew. Chem.* **2009**, *121*, 1048–1089; *Angew. Chem. Int. Ed.* **2009**, *48*, 1030–1069.
- [15] a) T. Moriuchi, S. Bandoh, M. Miyaishi, T. Hirao, *Eur. J. Inorg. Chem.* **2001**, 651–657; b) X. Shen, T. Moriuchi, T. Hirao, *Tetrahedron Lett.* **2004**, *45*, 4733–4736.
- [16] T. Moriuchi, M. Kamikawa, S. Bandoh, T. Hirao, *Chem. Commun.* **2002**, 1476–1477.
- [17] K. A. Connors, *Binding Constants*; Wiley, New York, **1987**.
- [18] B. Perlmutter-Hayman, *Acc. Chem. Res.* **1986**, *19*, 90–96.
- [19] For review on synthetic allosteric systems, see: a) L. Kovbasyuk, R. Krämer, *Chem. Rev.* **2004**, *104*, 3161–3187; b) M. Takeuchi, M. Ikeda, A. Sugasaki, S. Shinkai, *Acc. Chem. Res.* **2001**, *34*, 865–873; c) S. Shinkai, M. Ikeda, A. Sugasaki, M. Takeuchi, *Acc. Chem. Res.* **2001**, *34*, 494–503.
- [20] For recent synthetic allosteric systems, see: a) R. Wakabayashi, T. Ikeda, Y. Kubo, S. Shinkai, M. Takeuchi, *Angew. Chem.* **2009**, *121*, 6795–6798; *Angew. Chem. Int. Ed.* **2009**, *48*, 6667–6670; b) J. Set-sune, K. Watanabe, *J. Am. Chem. Soc.* **2008**, *130*, 2404–2405; c) H. J. Yoon, J. Heo, C. A. Mirkin, *J. Am. Chem. Soc.* **2007**, *129*, 14182–14183; d) T. Ikeda, O. Hirata, M. Takeuchi, S. Shinkai, *J. Am. Chem. Soc.* **2006**, *128*, 16008–16009; e) W.-H. Huang, S. Liu, P. Y. Zavalij, L. Isaacs, *J. Am. Chem. Soc.* **2006**, *128*, 14744–14745; f) J. L. Sessler, E. Tomat, V. M. Lynch, *J. Am. Chem. Soc.* **2006**, *128*, 4184–4185; g) B. Botta, F. Caporuscio, D. Subissati, A. Tafi, M. Botta, A. Filippi, M. Speranza, *Angew. Chem.* **2006**, *118*, 2783–2786; *Angew. Chem. Int. Ed.* **2006**, *45*, 2717–2720.
- [21] M. Ikeda, Y. Kubo, K. Yamashita, T. Ikeda, M. Takeuchi, S. Shinkai, *Eur. J. Org. Chem.* **2007**, 1883–1886.
- [22] a) P. N. Taylor, H. L. Anderson, *J. Am. Chem. Soc.* **1999**, *121*, 11538–11545; b) C. A. Hunter, S. Tomas, *J. Am. Chem. Soc.* **2006**, *128*, 8975–8979.
- [23] a) C. Y. Yang, Y. Cao, P. Smith, A. J. Heeger, *Synth. Met.* **1993**, *53*, 293–301; b) Y. Xia, J. M. Wiesinger, A. G. MacDiarmid, *Chem. Mater.* **1995**, *7*, 443–445; c) J. Joo, Y. C. Chung, H. G. Song, J. S. Baeck, W. P. Lee, A. J. Epstein, A. G. MacDiarmid, S. K. Jeong, E. J. Oh, *Synth. Met.* **1997**, *84*, 739–740; d) H. Yan, T. Ohta, N. Toshima, *Macromol. Mater. Eng.* **2001**, *286*, 139–142; e) Y. Long, Z. Chen, N. Wang, J. Li, M. Wan, *Physica B* **2004**, *344*, 82–87; f) I. Sasaki, J. Janata, M. Josowicz, *Polym. Degrad. Stab.* **2007**, *92*, 1408–1416.
- [24] D. Jeon, J. Kim, M. C. Gallagher, R. F. Willis, *Science* **1992**, *256*, 1662–1664.
- [25] We measured the conductivity of **3-EB** complexes by means of four-point probe technique. We could not evaluate the value (the resistivity was over 200 m Ω m); this means that the Pd complex does not act as a dopant just as the acid does, although we cannot rule out the possibility that *tert*-butyl substituent in **3** perturbs the conductivity in **EB**.
- [26] G. Chessa, A. Scriveranti, *J. Chem. Soc. Perkin Trans. 1* **1996**, 307–311.
- [27] Y. Kubo, M. Ikeda, A. Sugasaki, M. Takeuchi, S. Shinkai, *Tetrahedron Lett.* **2001**, *42*, 7435–7438.
- [28] A.-M. Fuller, D. A. Leigh, P. J. Lusby, I. D. H. Oswald, S. Parsons, D. B. Walker, *Angew. Chem.* **2004**, *116*, 4004–4008; *Angew. Chem. Int. Ed.* **2004**, *43*, 3914–3918.

Received: August 20, 2009

Published online: November 2, 2009